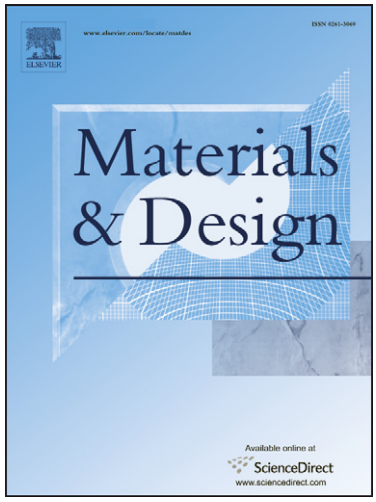

Sensitivity study on some parameters in blank design

M.C. Oliveira, R. Padmanabhan, A.J. Baptista, J.L. Alves, L.F. Menezes

PII: S0261-3069(08)00270-7
DOI: 10.1016/j.matdes.2008.06.010
Reference: JMAD 1957

To appear in: *Materials and Design*

Received Date: 10 April 2008
Accepted Date: 4 June 2008

Please cite this article as: Oliveira, M.C., Padmanabhan, R., Baptista, A.J., Alves, J.L., Menezes, L.F., Sensitivity study on some parameters in blank design, *Materials and Design* (2008), doi: 10.1016/j.matdes.2008.06.010

SENSITIVITY STUDY ON SOME PARAMETERS IN BLANK DESIGN

M.C. Oliveira[1], R. Padmanabhan[1]*, A.J. Baptista[1], J.L. Alves[2], L.F. Menezes[1]

[1]CEMUC, Centro de Engenharia Mecânica da Universidade de Coimbra, Faculty of Sciences and Technology, University of Coimbra, Polo II, Pinhal de Marrocos, 3030-201, Coimbra, Portugal

[2]Department of Mechanical Engineering, School of Engineering, University of Minho, Campus de Azurém, 4800-058, Guimarães, Portugal

*e-mail: padmanabhan@dem.uc.pt

Abstract

Sensitivity study on various numerical parameters is necessary for modeling a process. It is important to determine the influence of such parameters in order to achieve robust design. Initial blank shape is a process parameter that controls the quality of a formed part. This paper describes a blank shape optimization procedure that uses three numerical tools to determine an optimal blank shape for a formed part. Several numerical parameters that affect the optimization procedure for a deep drawn rectangular cup are analyzed. The focus is mainly on the influence of numerical parameters concerned with the use of NURBS surface in the optimization procedure. From the study, it is evident that the blank shape optimization procedure is sensitive to those numerical parameters. A significant influence of element size and optimization damping factor on achieving optimal blank shape is observed. The number of control points in the NURBS surface and the initial geometry have marginal influence on the optimization procedure.

Keywords: Sensitivity, blank design, optimization, FEM

1. Introduction

Advances in computing facilities have provided a solid platform for process analysis and immense applicability of these systems in simulating different process conditions. Therefore in recent times, researchers focus on numerical study because it provides insights on the material behaviour during forming processes. It enables the designer to optimize process and material parameters based on the requirements. Finite element method is a popular approach used in engineering practices for numerical modeling of physical systems and prediction of their behaviour under different conditions. The parameters used in the FE analysis may influence the solution outcome and hence a sensitivity study on the numerical parameters is important for accurate modeling. In sheet metal forming, a number of material and process parameters influence the flow characteristics of the blank and hence the quality of the part. Deep drawing is a sheet metal forming process that involves complex deformation behaviour of the blank due to large drawing ratio and shape of the part. Complexity grows multi-fold while modeling deep drawing process due to various assumptions made before modeling the process. For example, the friction contact conditions change during deep drawing but on contrary it is generally assumed to remain constant while modeling. Such assumptions significantly change the solution outcome and hence care should be taken while modeling deep drawing process. Apart from this, accurate prediction of the deformation behaviour depends on the material description [1-3]. In addition, several numerical parameters greatly influence the prediction of the deep drawing process [4, 5]. Therefore, these parameters are expected to influence blank shape optimization procedure as well. The optimization procedure presented is used to determine

an optimal blank shape for the cup based on the deformation behaviour of the blank during deep drawing process [6]. Three numerical tools, DD3IMP [7], DD3TRIM [8], and NURBS surface [9], are used in the optimization procedure. Deep drawing simulations were carried out using the in-house implicit finite element code DD3IMP. DD3IMP is specifically developed to simulate sheet metal forming processes. DD3TRIM is a numerical tool developed to trim solid finite element meshes. The trimming operation is performed based on a NURBS surface. Some numerical parameters related to the NURBS surface used in the optimization procedure are analyzed. Additionally, the factors used in the procedure and the finite element mesh constituting the blank are also analyzed.

2. Blank Shape Optimization Procedure

The blank shape optimization procedure is illustrated in Figure 1. An initial blank shape is selected or determined based on empirical formulae [10], and a corresponding NURBS surface is produced. A base mesh is cut with the initial NURBS surface to produce the initial finite element mesh. The base mesh is an uniform in-plane finite element mesh used to eliminate the typically necessary remeshing procedure. Combining this base mesh with DD3TRIM, the global FE in-plane element size is kept constant during the optimization procedure. This mesh is subjected to deep drawing simulation. The flange contour of the formed part is compared with the required target contour. If the flange contour is different from target contour, depending on its deviation, the initial NURBS surface is corrected and a new NURBS surface is produced. This new NURBS surface is used to trim the base mesh to produce intermediate blank shape which is subjected to deep drawing process. This procedure is repeated until the deviation between flange contour and target contour falls

below a user defined value "δ".

Figure 1, Blank shape optimization procedure.

2.1 Selected example: Rectangular cup

Figure 2 shows the geometry of the rectangular cup used in this study. The optimization procedure, to achieve the required flange contour (target), is based on the deformation history of the blank. The properties of mild steel (DC06) is used in this study. The work-hardening behaviour is considered isotropic and described by the Swift power law: $\bar{\sigma} = K\left(\varepsilon_0 + \bar{\varepsilon}^P\right)^n$, with the plastic anisotropy described by the Hill48´s quadratic yield criterion [11]. The elastic properties are: Young's Modulus E = 210 GPa, and Poisson ratio υ = 0.3. 0.2% proof strain ε_0 = 0.00439, $\bar{\sigma}$ is the flow stress and $\bar{\varepsilon}^p$ is equivalent plastic strain. The hardening parameters are: strength coefficient K = 529.5 MPa, and the strain-hardening exponent n = 0.268. The initial blank is 0.8 mm thick and the base mesh depicting the blank has 2 layers of 8 node solid finite elements through thickness. The deep drawing process parameters like, the tools geometry, the mechanical properties of the blank, the friction conditions and the blank holder force remain the same during the optimization procedure. Figure 3 shows the trajectory of nodes closest to the control points defining the initial NURBS surface, which is used to produce the initial finite element mesh, during the first deep drawing simulation. The positions of nodes are drawn at intervals of 5 mm starting from 10 mm of punch displacement. The trajectories of the nodes remain almost a straight line during deep drawing. Hence, in the correction stage of the blank shape optimization procedure, the movement of each node is assumed to follow a

straight line. This forms the basis for the vector used to determine the spatial distances between points of interest.

Figure 2, Geometry of the rectangular cup

Figure 3. Trajectory of nodal points during deep drawing

A simple and straightforward algorithm is used to compare the profile of the flange with the required target contour. In this particular case of the rectangular cup, three lines (1-3) define the target contour, as indicated in the figure 4. Straight line equations $(y = 30; \text{for } x < 26 \;\&\; x = 45; \text{for } y < 11)$ for lines 1 and 3, respectively, and the circle equation $[(x - 26)^2 + (y - 11)^2 = (19)^2]$ for line 2, are used in the algorithm to define the target contour. Only the first quadrant of the circle equation is considered for computing deviations across line 2.

Figure 4, Computation of deviation of nodal points

The procedure is based on the base mesh trimmed by the initial NURBS surface. At the end of each simulation, the closest nodes to the control points of the NURBS surface are identified. The straight line between its initial location ($\mathbf{X}^{\text{ini}}$) and final location ($\mathbf{X}^{\text{final}}$) is computed. Depending on the final position ($\mathbf{X}^{\text{final}}$) of the node along the periphery of the deformed blank, correction is made on the initial blank shape by relocating the control point. This line intersects the target contour at a point $\mathbf{X}^{\text{inter}}$, as illustrated in the figure with two different cases. Based on these three points, the corrected position of the border point Q, defining the new NURBS surface, is computed, as followed.

$$\mathbf{Q}_k = \mathbf{X}_k^{\text{init}} + \xi\left(\mathbf{X}_k^{\text{inter}} - \mathbf{X}_k^{\text{final}}\right) \text{ with } k = 1,2,3 \text{ and } \xi \in [0,1] \qquad (1)$$

Where `ξ´ is the damping factor used to control convergence characteristics of the optimization algorithm.

2.2. Shape Error

In order to quantify the deviation between the flange and the target contours, a geometrical measure namely, geometrical shape error, is used. Geometrical shape error (GSE), expressed in mm, is defined as the root mean square of the shape difference between the target shape and the deformed shape as in the following equation [12]:

$$\mathrm{GSE} = \sqrt{\frac{1}{n}\sum_{i=1}^{n}\left|\mathbf{X}^{\mathrm{inter}} - \mathbf{X}^{\mathrm{final}}\right|^2} \qquad (2)$$

The distance between $\mathbf{X}^{\mathrm{init}}$ and $\mathbf{X}^{\mathrm{final}}$ is evaluated at the end of each simulation, and n is the number of control points used in the initial and subsequent NURBS surfaces. When the GSE reaches a value less than "δ", a value predetermined by the user for a required accuracy in the flange shape, the iterative procedure is stopped because the optimal blank shape for the part has already been obtained.

The GSE allows correct estimation of the distance between the actual flange contour and the target contour. However, by definition it is not possible with GSE to evaluate whether the actual flange contour is more inside or outside the target contour. To clearly understand the shape error, a measure called target shape error (TSE) is used to quantify the deviation of the flange contour from the required target contour. Target shape error, also expressed in mm, is defined by the following equation:

$$\mathrm{TSE} = \frac{1}{n}\sum_{1}^{n} f\left(\frac{\left|\mathbf{X}^{\mathrm{init}} - \mathbf{X}^{\mathrm{final}}\right|}{\left|\mathbf{X}^{\mathrm{init}} - \mathbf{X}^{\mathrm{inter}}\right|}\right)\left|\mathbf{X}^{\mathrm{inter}} - \mathbf{X}^{\mathrm{final}}\right| \qquad (3)$$

$$\text{Where } f\left(\frac{\left|\mathbf{X}^{\text{init}}-\mathbf{X}^{\text{final}}\right|}{\left|\mathbf{X}^{\text{init}}-\mathbf{X}^{\text{inter}}\right|}\right)=\begin{Bmatrix} 1 \quad \text{if} \quad \dfrac{\left|\mathbf{X}^{\text{init}}-\mathbf{X}^{\text{final}}\right|}{\left|\mathbf{X}^{\text{init}}-\mathbf{X}^{\text{inter}}\right|} < 1 \Rightarrow \text{Outside the target} \\ -1 \quad \text{if} \quad \dfrac{\left|\mathbf{X}^{\text{init}}-\mathbf{X}^{\text{final}}\right|}{\left|\mathbf{X}^{\text{init}}-\mathbf{X}^{\text{inter}}\right|} < 1 \Rightarrow \text{Inside the target} \end{Bmatrix}$$

The TSE allows correct estimation of the distance between the actual flange contour and the target contour and to determine the total deviation.

3. Sensitivity study on numerical parameters

3.1. FE mesh size

Finite element size is a numerical parameter that, generally, has greater influence on the solution outcome. A fine mesh can produce accurate results compared to a coarse mesh. But, fine meshes render problems in the computational requirements needed to analyze the model. Hence, a designer should strike a balance with the finite element size to have a closer accuracy for optimal computational requirements. To study the effect of mesh refinement, several analyses were carried out for base mesh in-plane element sizes ranging between 0.8, 1.0, 1.25, 1.38, 1.5, 2 mm. The objective is to determine the optimal element size for the chosen geometry. The base mesh is trimmed using a NURBS surface with a radius of 60 mm. Figure 5 shows the punch force as a function of punch displacement for different element sizes. Smaller element size of 0.8 mm predicts less punch force compared to an element size of 2.0 mm. All other element sizes predict punch forces bound between these values, as indicated in the figure. It is evident that the element size has moderate influence on the punch force which proportionally decreases with the decrease in element size.

Figure 5, Influence of element size on the punch force

Figure 6, (a) Geometric shape error in the flange, (b) Draw-in along OX

Figure 6 (a) shows the GSE after one iteration for the different in-plane finite element sizes. Marginal increase in the GSE is observed which is due to the flow behaviour of the finite elements. Due to their size, smaller elements posses increased bending behaviour and hence flow a little more than larger elements. This leads to the difference in the overall draw-in and hence geometric shape error. Since the difference in draw-in is marginal among the range of in-plane finite element sizes studied, a point on the flange periphery along the OX axis was picked to quantify the draw-in. Figure 6 (b) shows the location of those points along the OX axis for different element sizes to illustrate draw-in. The draw-in is more for smaller in-plane finite element sizes and reduces as the element size increases. Large element size leads to larger inaccuracies. Saturation in the draw-in was observed in 3 middle element sizes (1.25, 1.38, & 1.5 mm) at this particular point.

Figure 7 (a) shows the equivalent tensile stress-equivalent tensile strain history at a critical point in the cup corner. The stress reduces moderately with the reduction in the in-plane finite element size. It is clear that an in-plane finite element size greater than 1.5 mm is not sufficient for an accurate representation of the deep drawing process. This is in agreement with other authors results that indicate that the in-plane finite element size must correspond to a contact turning angle of approximately 5º (in this case 1.25 mm) [13, 14].

Figure 7, (a) Eqv. tensile stress-strain curve, (b) Simulation time for different element sizes

Even with the results presented above, in the chosen range of element sizes, it is difficult to conclude that one in-plane finite element size is best suitable for the described geometry. The accuracy of the properties estimation increased as the in-plane finite element size reduced. On contrary, the time required to solve the system increased exponentially. Figure 7 (b) shows the computation time taken for each simulation for different in-plane finite element sizes. As the point of inflection indicates, 1.38 mm element size was found to be optimal for selected geometry, striking a balance between accuracy and efficiency.

3.2. Initial geometry

Two different geometries were chosen to determine the influence of initial geometry on the blank shape optimization procedure. The circular blank used in the previous section and a blank shape produced from empirical formulae, presented in figure 8 (a), were studied. In the initial stages, the target shape error strongly depends on the size of the initial blank with respect to the part geometry. The blank produced using empirical formulae is larger compared to the selected circular blank. Large initial blank resulted in large initial shape error as shown in figure 8 (b). The variation is significant in the initial stages and drastically reduces as the number of iterations increase. The difference in shape error estimate vanishes after 4 iterations as shown in the figure. This fact results from the use of a constant damping factor of 0.6 and its influence remains the same for both shape optimization scheme. To better understand this numerical parameter, the influence damping factor is analyzed in the next section.

Figure 8, (a) Blank shape produced using empirical formulae, (b) Influence of initial blank size on the shape error

3.3. Damping factor

Depending on the final position ($\mathbf{X}^{final}$) of the node on the periphery of the deformed blank, correction is made on the initial blank shape by relocating the control point. A damping factor `ξ´ is introduced in the correction algorithm since for $\xi = 1$, relocation of the control points resulted in strong flange contour oscillating between very large and very small values. The initial blank shape is produced from empirical formulae, corresponding to the initial contour presented in figure 8 (a). Due to its large initial error, several iterations were needed to achieve the optimal blank shape as shown in figure 9.

Figure 9, Influence of damping factor on TSE

The damping factor is applied to arrest this oscillation between extreme shapes, completely inside and completely outside target solutions. Figure 9 presents the TSE error evolution along the optimization procedure for different constant damping factors. Large target shape error observed in the first iteration and the flange contour oscillation thereafter (when $\xi =$ 0.8 & 1.0) is due to the large initial blank shape obtained from the empirical equations. Due to the large initial blank shape, for high values of the damping factor the correction stage leads to a strong variation of the initial blank shape. This explains why for every even iteration, and damping factors 0.8 and 1.0, the flange contour is located inside the target contour, at the end of the punch stroke. These oscillations between outside and inside of the target contour are clearly controlled by the damping factor. After the first iteration, the TSE reduced depending on the damping factor used in a scheme. A value of 1.0 (without damping) produced maximum TSE and hence took most number of iterations to arrive at an optimal blank shape. As indicated in the figure, using a damping factor of 0.6 in the

correction algorithm, after each simulation, results in fast convergence of shape error below user defined value. Even in the presence of over estimation of initial blank shape, the proposed algorithm is capable of achieving the optimal blank shape within four iterations, in the case of the studied rectangular cup deep drawing. The damping factor of 0.6 resulted in few iterations to achieve the optimal blank shape. This value seems to indicate that minimum iterations are guaranteed when the difference in the TSE error between two iterations is maximum, as long as no oscillations occur. Since it could be expected to improve convergence by adopting an evolutionary damping factor, the impact of changing the damping factor during blank shape optimization procedure is studied by using combinations of two values, i.e., 0.6 (best damping factor, indicated by number 1) and 1.0 (worst damping factor, indicated by number 2).

The circular blank with 60 mm radius which results in lesser initial shape error, was used in this section. Figure 10 shows the evolution of geometrical shape error over iterations for an in-plane finite element size of 1.38 mm. Using a damping factor of 1.0 in every correction stage, after each iteration, resulted in large number of iterations to reach the user defined error limit, as described previously, and shown in figure 10. Combinations of damping factors between 0.6 and 1.0 reduced the iterations required to achieve the user defined error limit. However, the damping factor of 0.6 yield better result and hence it is used in the studies presented in following sections.

Figure 10, Effect of combining damping factors on achieving the user defined error limit

Similar study was carried out for different in-plane finite element sizes to determine the impact of the combination between the damping factor and the in-plane finite element size. Table 1 show the GSE´s, when using in-plane finite element sizes of 1.25 and 1.5 mm, for the same combinations of damping factors (between 0.6 and 1.0) as discussed previously. Apparently, little differences in the GSE are evident, demonstrating the negligible influence of in-plane finite element size on the solution convergence with respect to the damping factor. Especially after fourth iteration, as highlighted in the last two columns, the variation in geometric shape error using different element sizes becomes negligible demonstrating the robustness of the described blank shape optimization procedure.

Table 1, Evolution of GSE over iterations

3.4. Number of Control points

The deviation between the flange contour and the target contour is quantified using a set of points on the blank periphery, equations (2) and (3). Thus, the shape error estimation introduces a numerical parameter namely the number of control points defining the NURBS surface, to be included in the sensitivity study. More number of control points in the NURBS surface increases the solution accuracy because the flange contour is closely captured. The influence of the number of control points, defining the NURBS surface, on the TSE is studied in this section. Four different NURBS curves with different number of control points were used to determine their influence on achieving optimal initial blank shape for the rectangular cup. The first NURBS curve used in the previous studies was created using empirical equations and has 23 control points equally distributed over the length of the curve, rendering the initial contour presented in figure 3. This curve was then

simplified by removing the less significant knots to produce second NURBS curve, using knot removal technique [9]. By this technique, the less significant knots were removed and the positions for the reduced number of control points were calculated. Similarly, a third NURBS curve was produced by further simplifying the second NURBS curve. The second and the third NURBS curves are defined by 11 and 5 control points respectively. A fourth NURBS surface with 43 control points was produced by adding knots. Due to the density of the control points, the surface appeared as a line and hence it is not depicted here. Thus, four NURBS surfaces were used separately and interpolated based on flange geometry to produce intermediate blank shapes. Figure 11 (a) – (c) shows the three initial NURBS curves and their respective control points locations. As the number of control points reduces, the shape of the NURBS surface deviates from the original surface. The deviation is more pronounced in the NURBS surface with 5 control points, figure 11 (c).

Figure 11, NURBS surfaces with (a) 23, (b) 11, (c) 5 control points

Figure 12 (a) shows the evolution of target shape error over iterations for the 4 NURBS surfaces. In the first iteration, NURBS surface with 5 control points produced least error compared to surfaces with 11 and 23 control points. This error is a consequence of pronounced deviation of the NURBS surface from the original shape obtained from the empirical formulae. In fact, the initial surface is closer to the optimal blank shape that presents an elliptical shape. Thereafter the difference vanished indicating their insignificance in geometrical shape error estimation. The number of control points in the NURBS surface influences TSE, especially in the initial stages of blank shape optimization. For higher number of control points defining the NURBS surface results in higher influence

on the TSE. However, a refined NURBS surface describes the target contour closely and consequently the correction algorithm determines appropriate blank shapes. It allows the evaluation of the optimal blank shape without any influence in the computation time. When the number of control points defining the NURBS surface is less, the algorithm is insensitive to the admissible in-plane finite element size. The NURBS surface with 11 control points is tested with two in-plane finite element sizes, 0.8 mm and 1.38 mm. As shown in figure 12 (b), negligible difference in the target shape error is observed and is due to the far located control points. The trend in the convergence of TSE appeared similar to any other NURBS surfaces with different number of control points.

Figure 12, Convergence of TSE based on (a) No. of control points defining the NURBS surface,

(b) Element size with 11 control points defining the NURBS surface.

In addition to the number, the locations of control points also have significant influence on the shape error estimation. The distribution pattern of the 23 control points of the original NURBS surface presented in figure 8 (a) is changed, as shown in figures 13 (a) & (b). In one of the NURBS surface (S2), the control points were concentrated close to OX axis as more material flow is expected around this region. As shown in figure 13 (c), large difference in the target shape error was observed in the first iteration for surface S2, due to the concentration of control points. As more material flow occurs around this area, and more points are involved in determining the shape error, the shape error estimate also increased.

Figure 13, Effect of control points distribution on target shape error estimation

The difference between the shape error estimates reduces considerably from second iteration, but continues to be different until the end. This clearly indicates that the construction of NURBS surface and the geometry of the part are sensitive to the algorithm. However, the target shape error reduces below 1 mm within 4 iterations.

8. Summary

Sensitivity study on the influence of some numerical parameters was carried out for a blank shape optimization procedure. This is necessary for modeling deep drawing process in order to rightly predict the deformation behaviour of the blank. A blank shape optimization procedure using finite element method is discussed. The procedure uses three numerical tools and hence introduces a number of numerical parameters, some of which were studied in this paper. The damping factor used to contain the flange contour oscillation plays a major role in arriving at a solution within reasonable iterations. A value of 0.6 produced best result and value of 1.0 prolonged the procedure. The shape error estimation for a deep drawn part is significantly influenced by the number of control points defining the NURBS surface used in the procedure. In addition, the location and distribution of the control points on the flange periphery also influences the shape error estimation. Even with these influencing factors, the described blank shape optimization procedure is capable of determining the optimal blank shape within four iterations.

9. Acknowledgement

The authors are grateful to the Portuguese Foundation for Science and Technology (FCT) for the financial support for this work, through the Program POCI 2010.

10. References

[1] Hopperstad OS, Berstad T, Ilstad H, Lademo OG, Langseth M. Effects of the yield criterion on local deformations in numerical simulation of profile forming, Journal of materials processing technology. 1998; 80-81:551-555.

[2] Moreira LP, Ferron G, Ferran G. Experimental and numerical analysis of the cup drawing test for orthotropic metal sheets. Journal of materials processing technology. 2000;108:78-86.

[3] Bouvier S, Alves JL, Oliveira MC, Menezes LF. Modelling of anisotropic work-hardening behaviour of metallic materials subjected to strain-path changes. Computational Materials Science. 2005;32:301-315.

[4] Laurent Duchêne, Habraken AM. Analysis of the sensitivity of FEM predictions to numerical parameters in deep drawing simulations. European Journal of Mechanics A/Solids. 2005;24:614-629.

[5] Amit Jaisingh, Narasimhan K, Date PP, Maiti SK, Singh UP. Sensitivity analysis of a deep drawing process for miniaturized products. Journal of Materials Processing Technology. 2004;147:321-327.

[6] Padmanabhan R, Baptista AJ, Oliveira MC, Tekaya M, Dogui A, Salah BH, Alves JL, Menezes LF. Blank shape optimization using parametric NURBS surfaces. Proceedings of IDDRG´06, June 2006, Edited by Abel D. Santos, A. Barata da Rocha, Porto, Portugal.

[7] Menezes LF, Teodosiu C. Three-dimensional numerical simulation of the deep-drawing process using solid finite elements. Journal of Materials Processing

Technology. 2000;97:1-3:100-106.

[8] Baptista AJ, Alves JL, Rodrigues DM, Menezes LF. Trimming of 3D solid finite element meshes using parametric surfaces: Application to sheet metal forming. Finite Element Analysis and Design. 2006;42:12:1053-1060.

[9] Les Piegl, Wayne Tiller, The NURBS Book, 2nd Edition, Springer-Verlag Berlin, 1997.

[10] Barata da Rocha, Ferreira Duarte J. Technolgia da Embutidura, Edited by Associação Portuguesa das Tecnologias de Conformação Plástica (APTCP), 1993.

[11] Hill R. A theory of the yielding and plastic flow of anisotropic metals, Proceedings of the Royal Society, London A. 1948; 193:281-297.

[12] Park SH, Yoon JW, Yang DY, Kim YH. Optimum blank design in sheet metal forming by the deformation path iteration method. International Journal of Mechanical Sciences. 1999;41:1217-1232.

[13] Li KP, Carden, WP, Wagoner RH. Simulation of springback. International Journal of Mechanical Sciences. 2002;44:103-122.

[14] Padmanabhan R, Oliveira MC, Baptista AJ, Alves JL, Menezes LF. Study on the influence of the refinement of a 3-D finite element mesh in springback evaluation of plane-strain channel sections. Proceedings of NUMIFORM'07. 2007; 847-852.

List of Figures

List of Tables

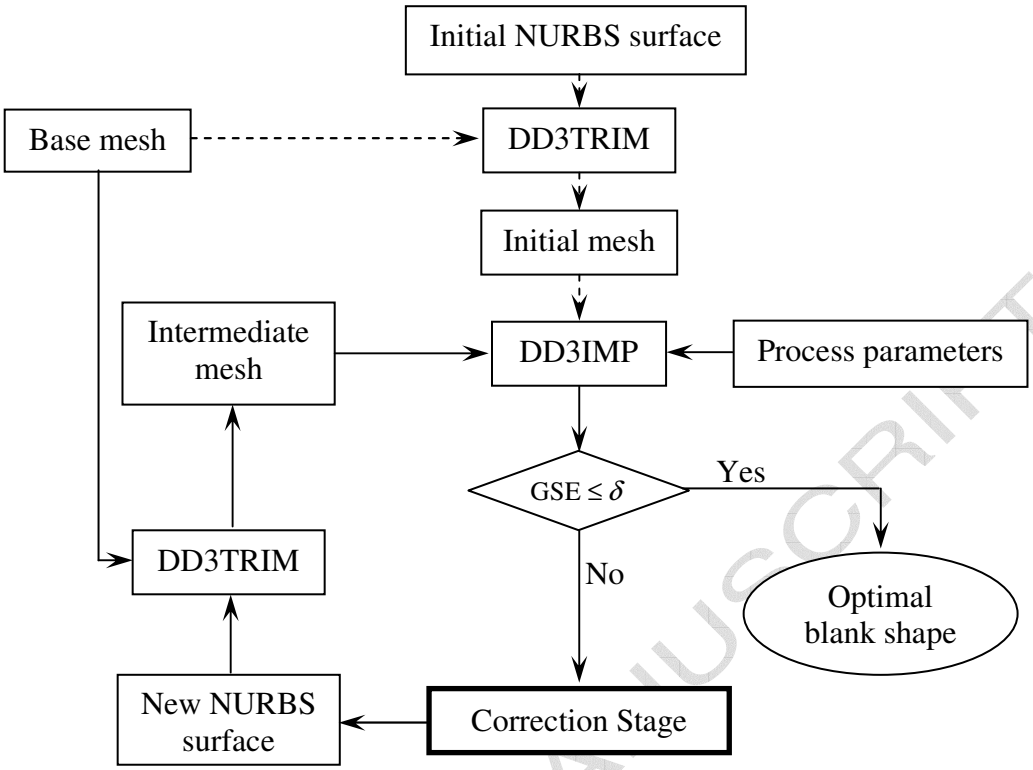

Figure 1, Blank shape optimization procedure.

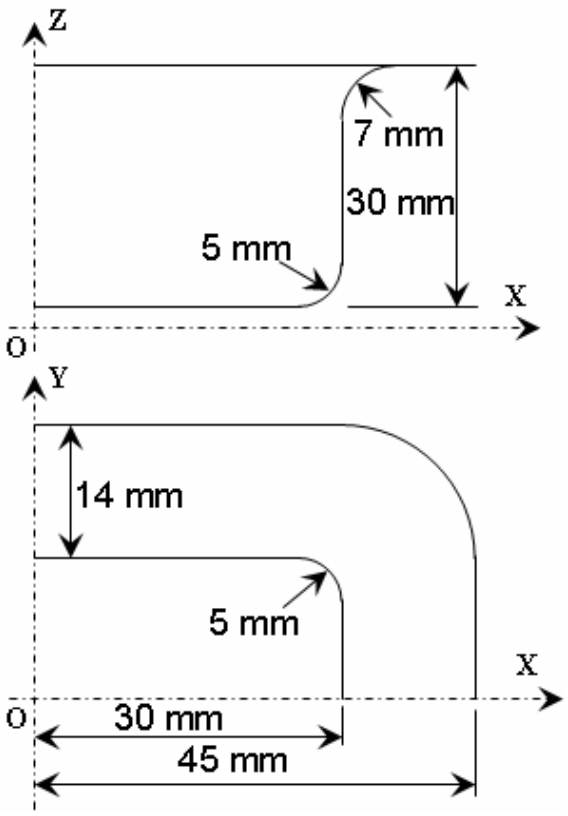

Figure 2, Geometry of the rectangular cup

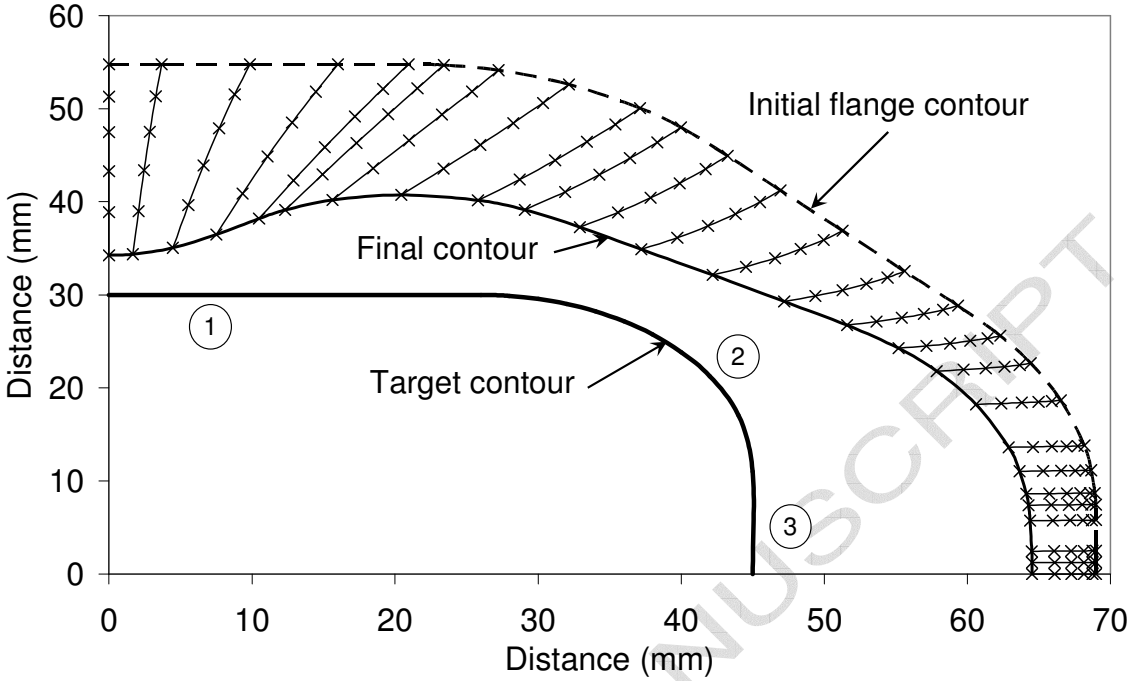

Figure 3. Trajectory of nodal points during deep drawing

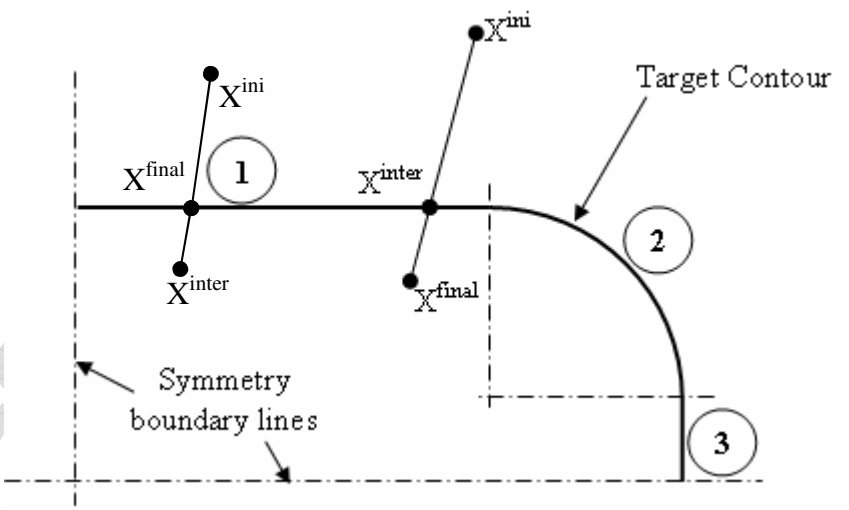

Figure 4, Computation of deviation of nodal points

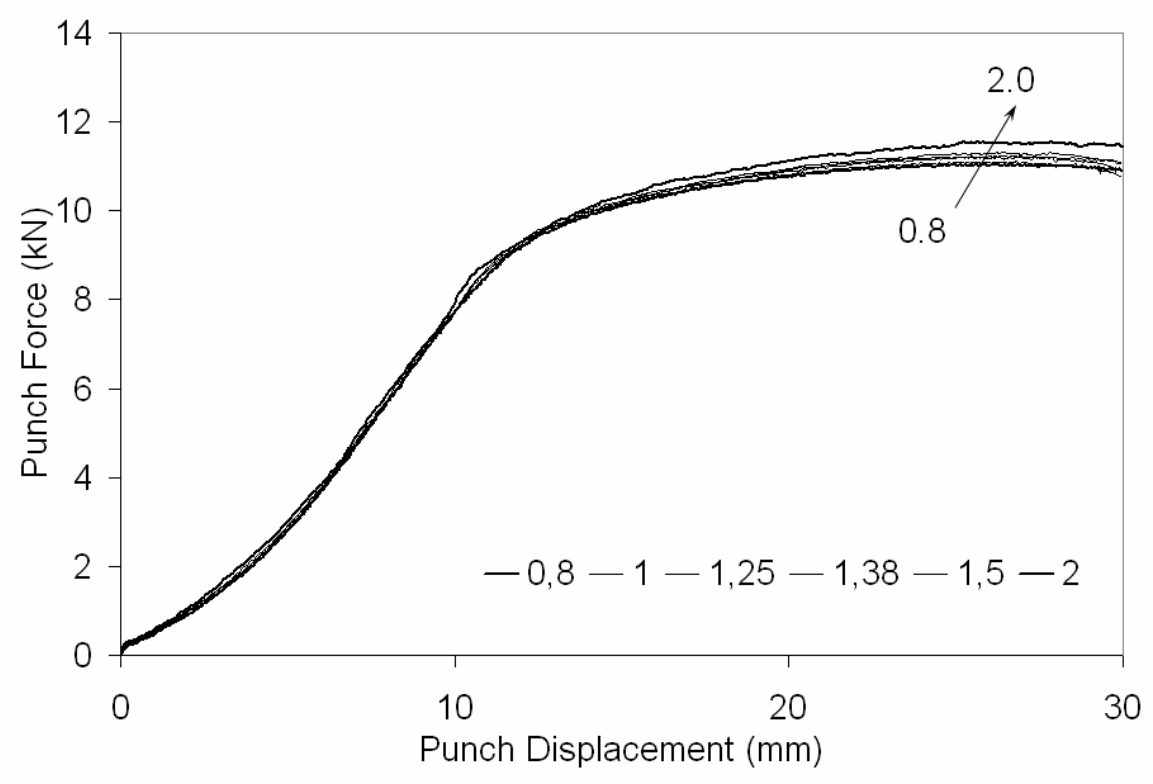

Figure 5, Influence of element size on the punch force

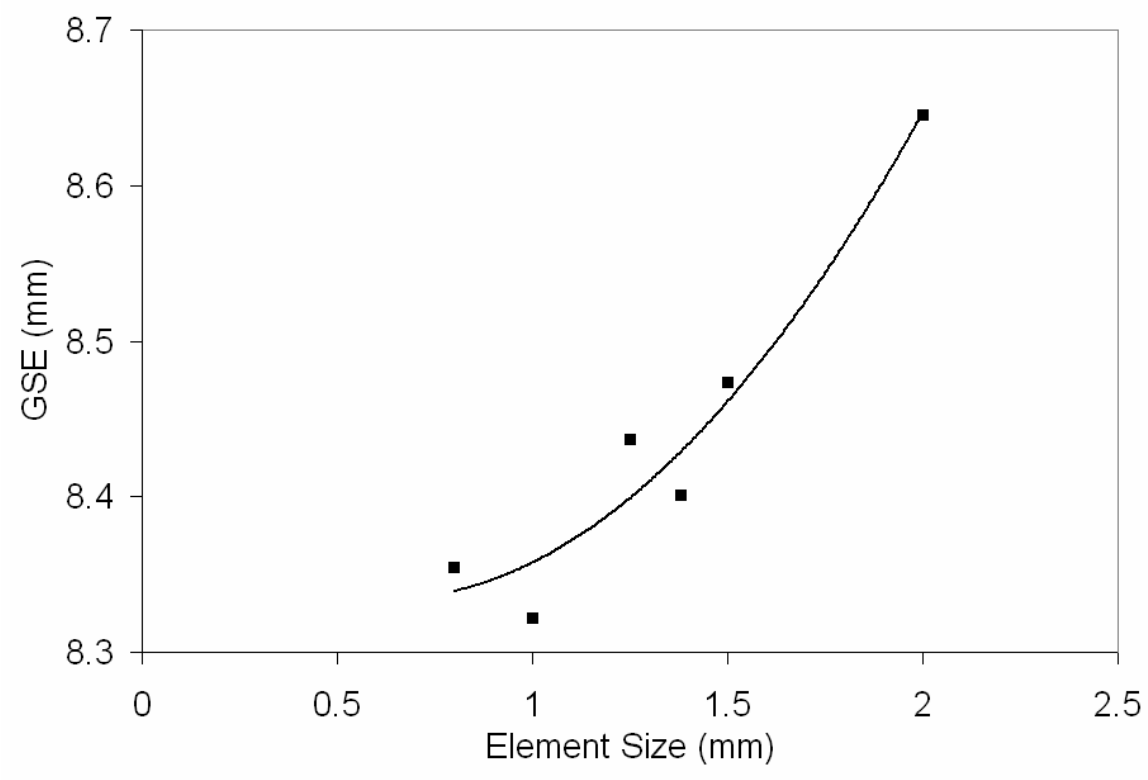

Figure 6, (a) Geometric shape error in the flange

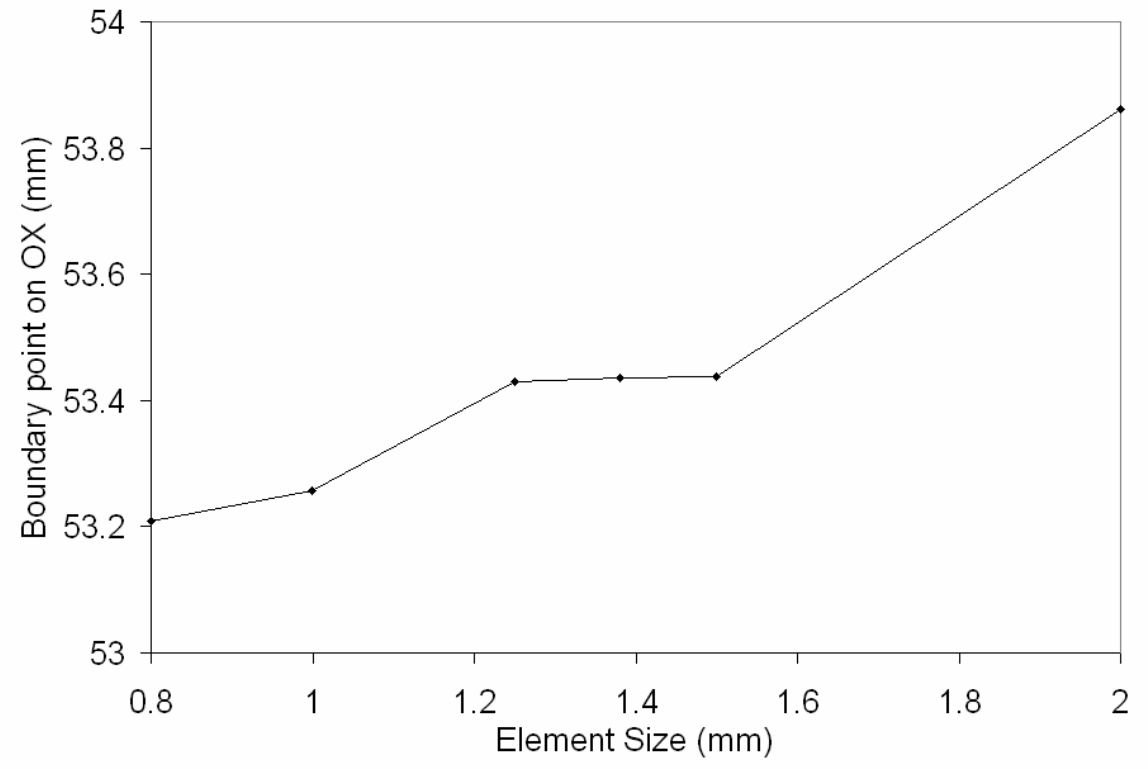

Figure 6, (b) Draw-in along OX

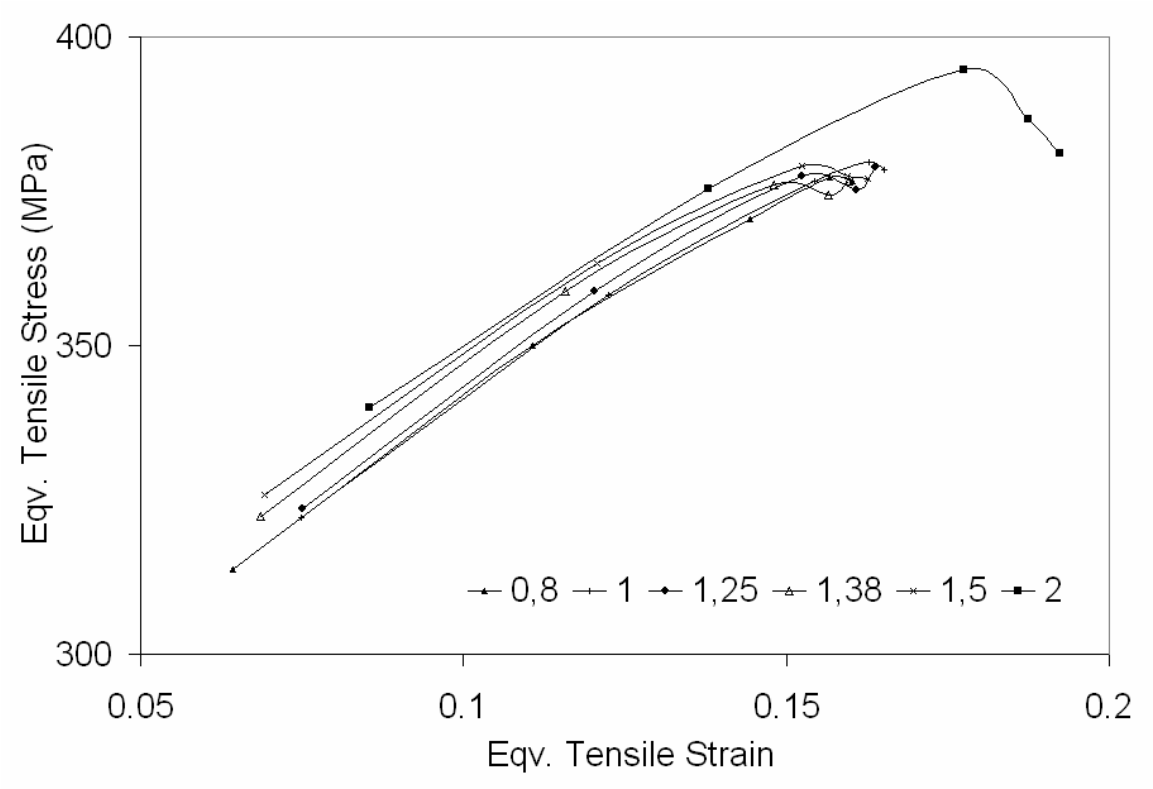

Figure 7, (a) Eqv. tensile stress-Eqv. tensile strain curve

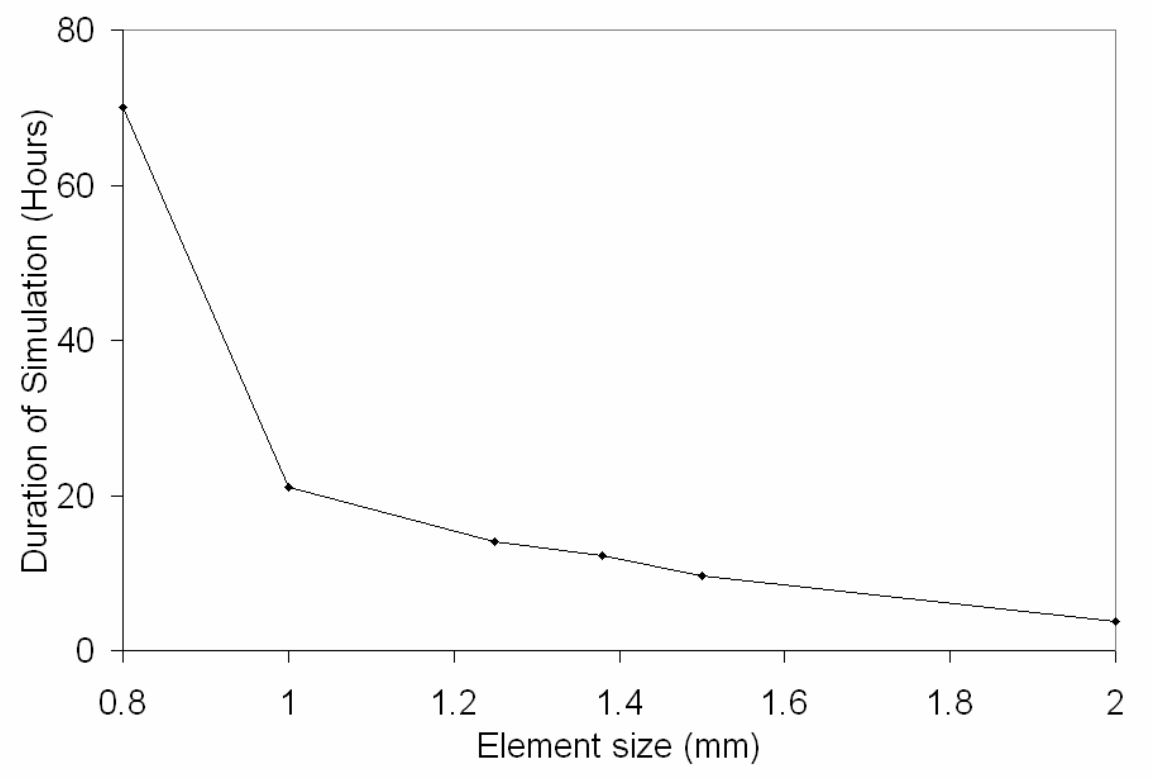

Figure 7, (b) Computation time for different element sizes

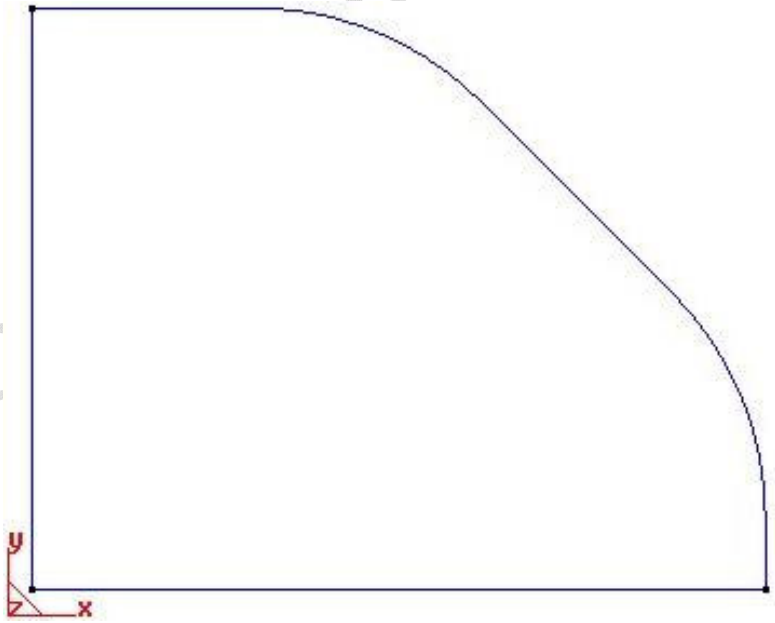

Figure 8, (a) Blank shape produced using empirical formulae

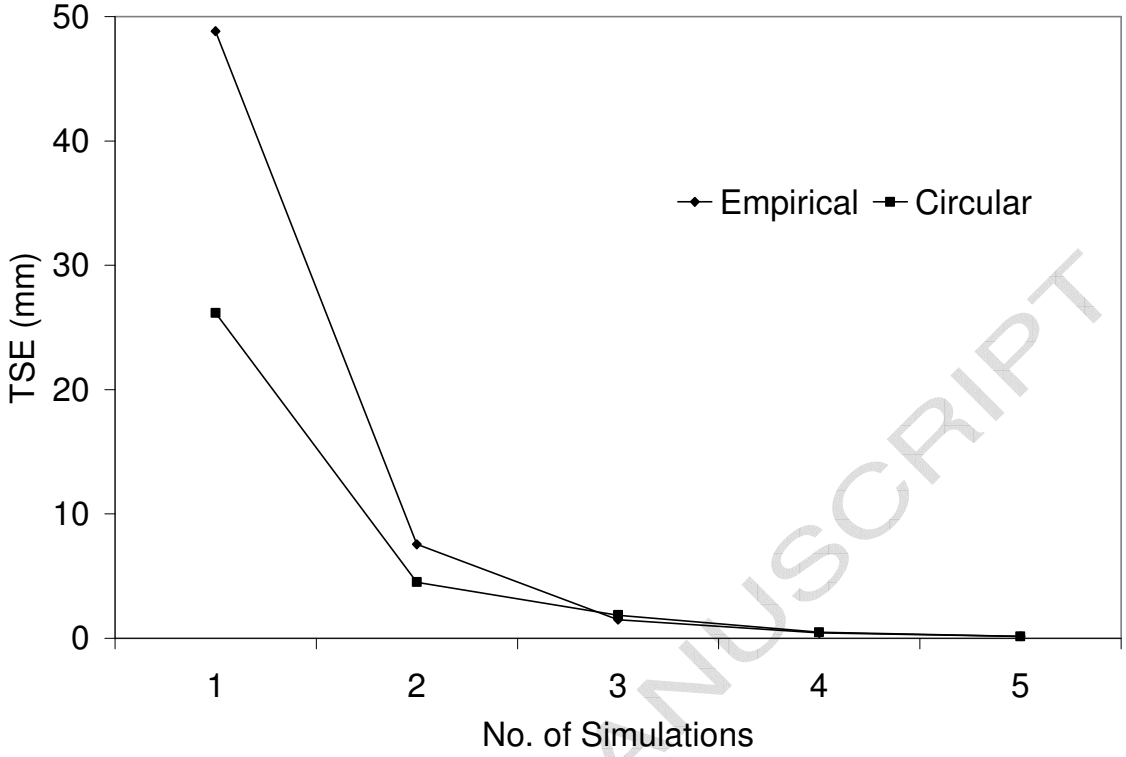

Figure 8, (b) Influence of initial blank size on the shape error

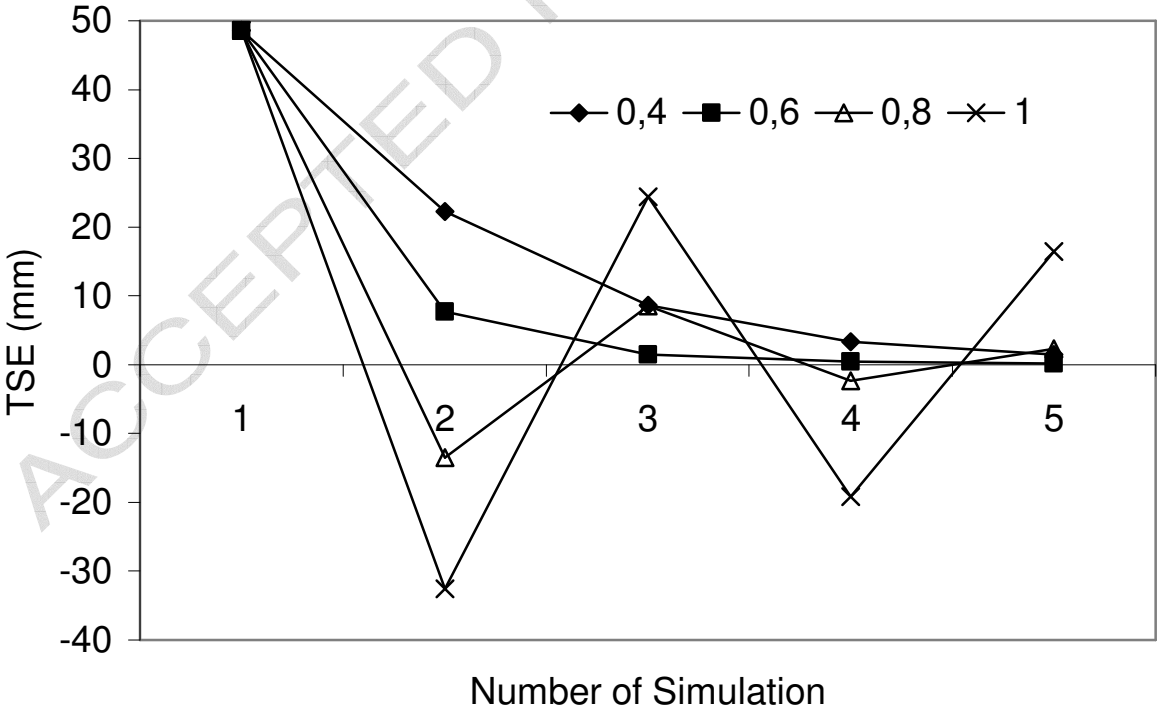

Figure 9, Influence of damping coefficient on TSE

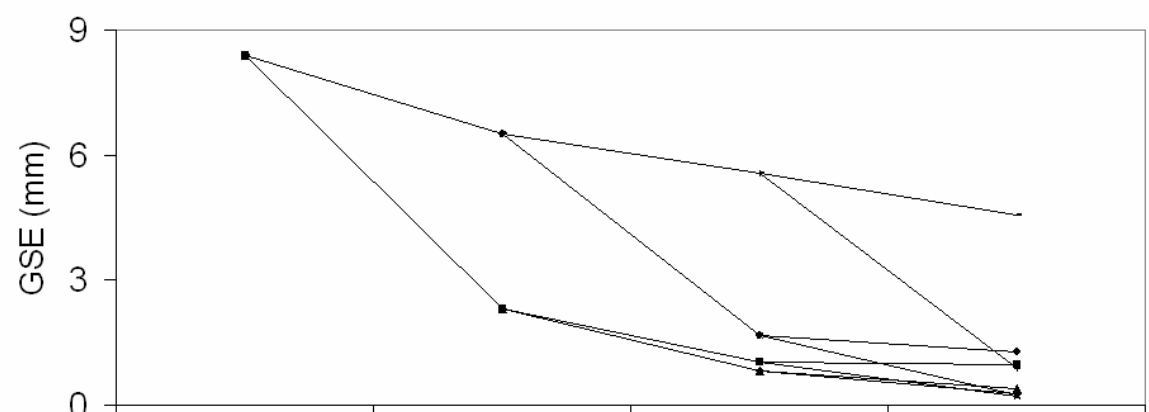

	1	2	3	4
111	8.4014	2.3077	0.8321	0.2601
122	8.4014	2.3077	1.0363	0.9765
112	8.4014	2.3077	0.8321	0.3864
121	8.4014	2.3077	1.0363	0.2095
211	8.4014	6.5082	1.6578	0.2338
212	8.4014	6.5082	1.6578	1.2855
221	8.4014	6.5082	5.5649	0.883
222	8.4014	6.5082	5.5649	4.5648

No. of Iterations

Figure 10, Effect of combining damping factors on achieving the user defined error limit

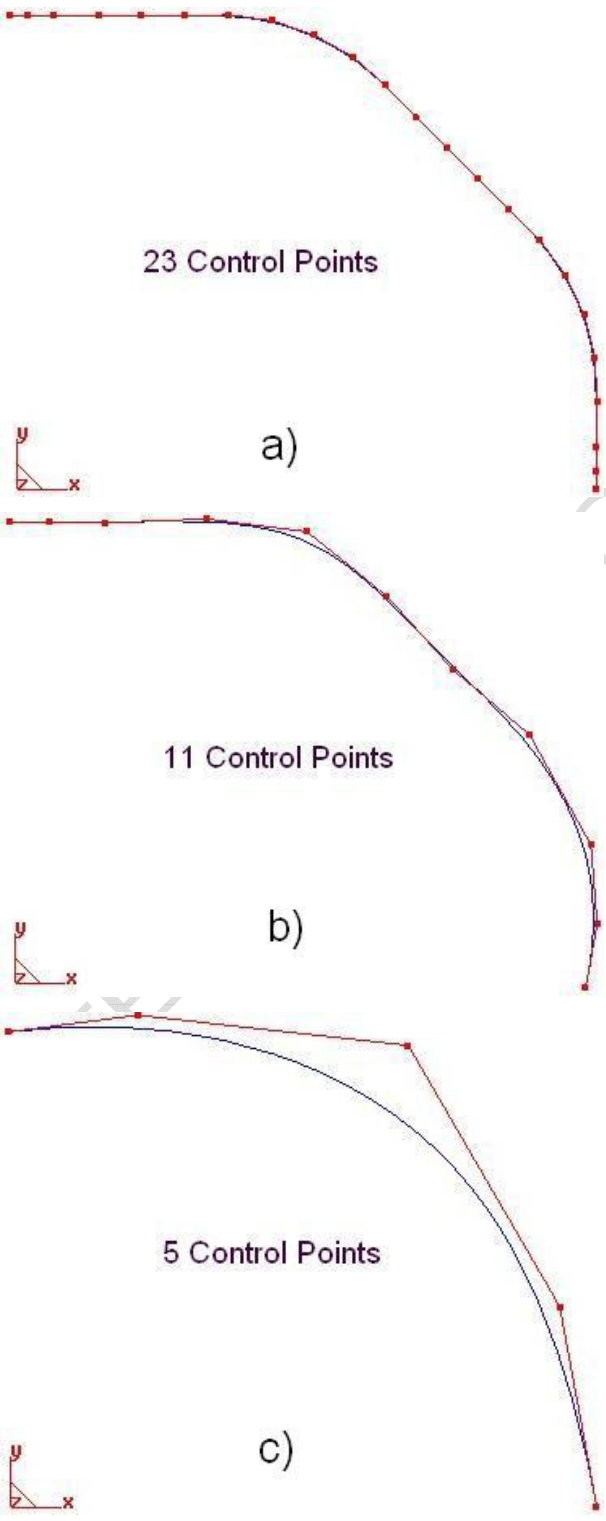

Figure 11, NURBS surfaces with (a) 23, (b) 11, (c) 5 control points

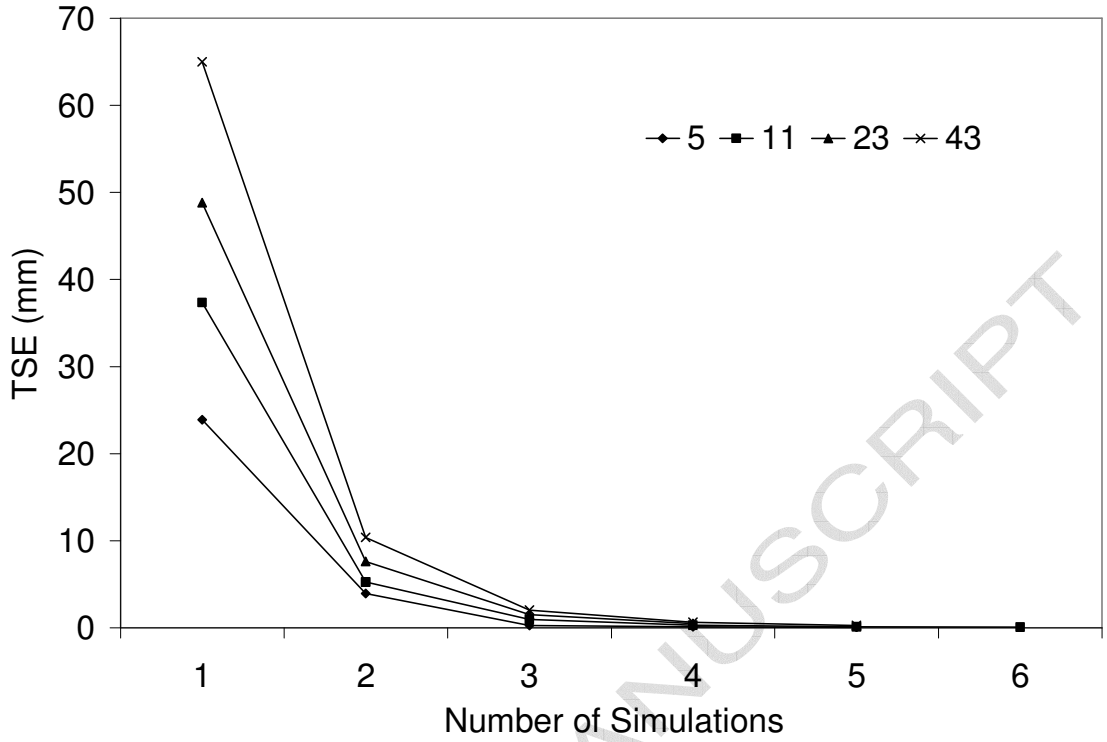

Figure. 12, Convergence of TSE based on (a) No. of control points defining the NURBS surface,

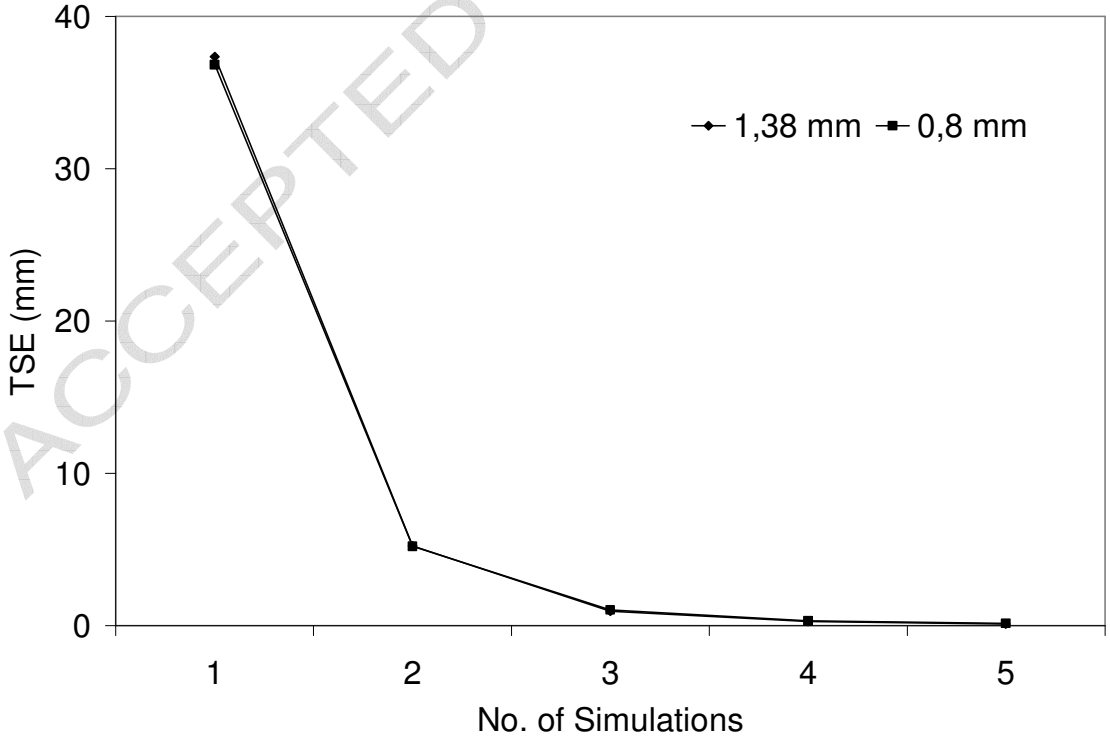

Figure 12 (b) Element size with 11 control points defining the NURBS surface.

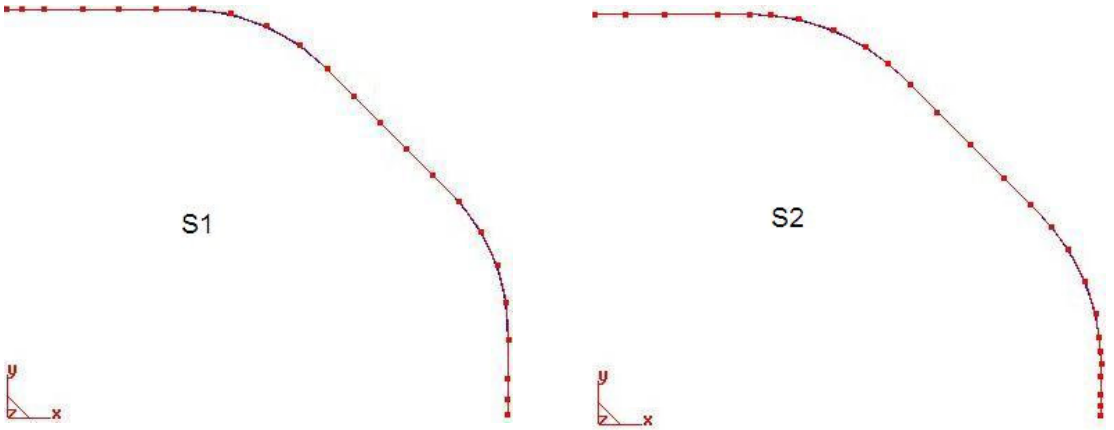

(a) (b)

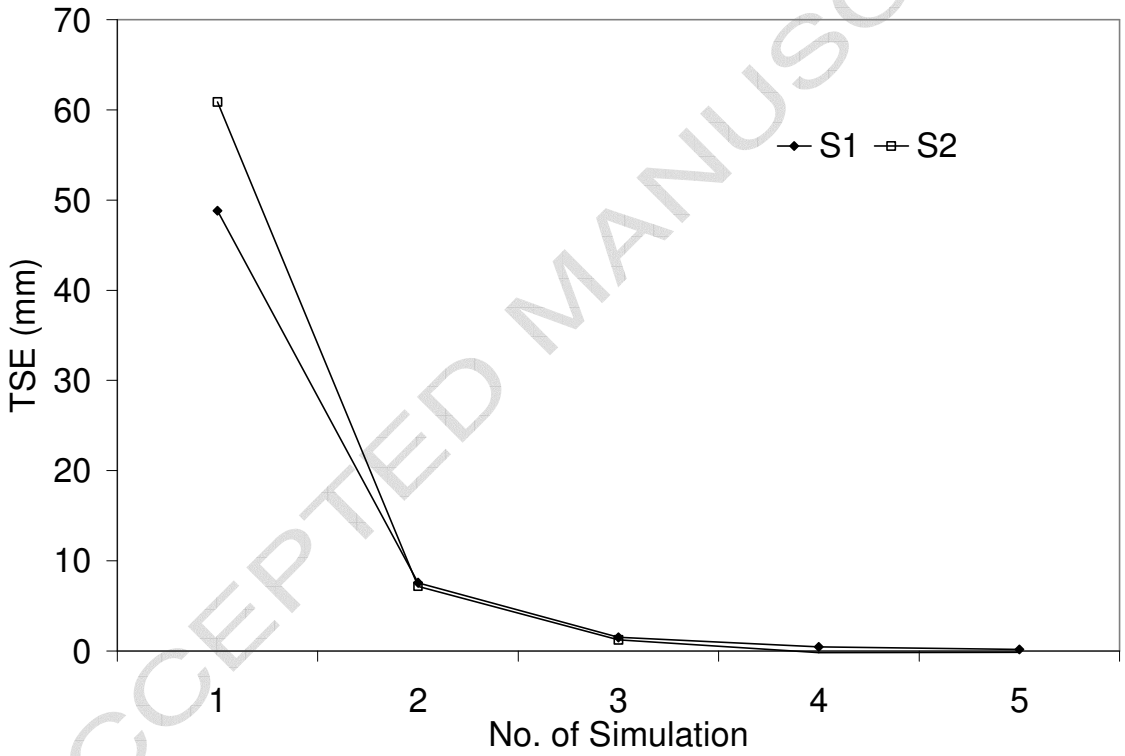

(c)

Figure 13, Effect of control points distribution on target shape error estimation

Table 1, Evolution of GSE over iterations

Damping factor combinations	Iteration 1		Iteration 2		Iteration 3		Iteration 4	
	1.25 mm	1.50 mm	1.25 mm	1.50 mm	1.25 mm	1.50 mm	1.25 mm	1.50 mm
111	8.4371	8.4739	2.2841	2.2971	0.8305	0.8202	**0.2560**	**0.2492**
122	8.4371	8.4739	2.2841	2.2971	1.0573	1.0298	**1.0536**	**0.9392**
112	8.4371	8.4739	2.2841	2.2971	0.8305	0.8202	**0.3816**	**0.3965**
121	8.4371	8.4739	2.2841	2.2971	1.0573	1.0298	**0.2146**	**0.1821**
211	8.4371	8.4739	6.5957	6.4800	1.6864	1.6375	**0.2511**	**0.2467**
212	8.4371	8.4739	6.5957	6.4800	1.6864	1.6375	**1.3305**	**1.2798**
221	8.4371	8.4739	6.5957	6.4800	5.2684	5.5433	**0.8984**	**0.8501**
222	8.4371	8.4739	6.5957	6.4800	5.2684	5.5433	**4.6986**	**4.2205**